Optimal Eye and Head Movement Control using q-parametrization [⋆]

Sanath Darshana Kahagalage [∗], **Eugenio Aulisa** [∗], **Bijoy K. Ghosh** [∗],

[∗] *Dept. of Mathematics and Statistics, Texas Tech University, Lubbock, TX, USA*

Abstract: Human eye and head movements can be looked at, as a rotational dynamics on the space **SO(3)** with constraints that have to do with the axis of rotation. Eye movements satisfy Listing's constraint, wherein the axis vector is restricted to a fixed plane called the Listing's plane. On the other hand, head movements satisfy Donders' constraint, wherein the axis vector, after a suitable scaling, is assumed to lie in a surface called Donders' surface. Various descriptions of the Donders' surface are in the literature and in this paper we assume that the surface originates from the Fick gimbal. Assuming boundary values on the states, optimal movement trajectories are constructed where the goal is to transfer the state between an initial to a final value while minimizing a quadratic cost function on the energy of the, externally applied, control torques. Using Newton-Euler formulation of the dynamical system, in this paper we introduce a new q-parametrization to synthesize the optimal control.

Keywords: Rigid body dynamics, Listing's law, Donders' law, Optimal Control, Quaternions

1. INTRODUCTION

Neurologists, physiologists and engineers have been interested in modeling and control of the eye since 1845 with notable studies conducted by Listing (1845), Donders (1848. Press, 1996) and Helmholtz (1866). Specifically, it has been observed that the oculomotor system chooses just one angle of ocular torsion for any one gaze direction (see Donders (1848. Press, 1996)). Since its discovery, the Donders' law has also been applied to the head (see Ceylan et al. (2000)), which is mechanically able to rotate torsionally, but which normally adopts just one torsional angle for any one facing direction, see Straumann et al. (1991), Glenn and Vilis (1992). A geometric consequence of the Donders' Law is that the three dimensional vectors that represent the 'rotation vectors' of the head are not spread out in a 3-D volume but instead fall in a single two-dimensional surface known as the Donders' surface. It has been further proposed, see Glenn and Vilis (1992), Theeuwen et al. (1993), Radau et al. (1994), Tweed et al. (1995), Medendorp et al. (1998), Misslisch et al. (1998), that Donders' Law follows what is known as the Fick's strategy. According to this strategy, Donders' surface is a saddle-shaped surface, with non-zero torsional components at oblique facing directions, obtained by mildly twisting a plane (see Fig. 1). Listing's law for eye movement follows precisely when the Donders' surface degenerates to a plane, i.e. when the torsional component of the rotation vector is zero.

2. BACKGROUND

Representation of 'eye and head orientations' using quaternions has already been described in Polpitiya et al. (2007), Ghosh and Wijayasinghe (2012a). We revisit some of the main ideas in this section. A quaternion is a four tuple of real numbers and the space of unit quaternions is identified with the unit sphere in $\mathbb{R}^4$ and denoted by S^3. To each $q \in S^3$ written as $q = (q_0, q_1, q_2, q_3)$,

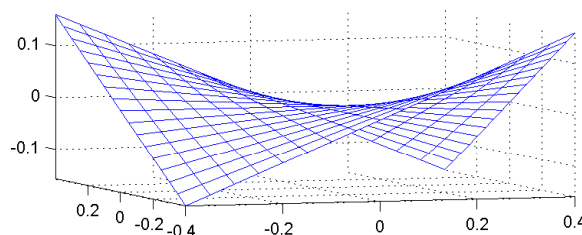[⋆] Corresponding author is Bijoy K. Ghosh.

Fig. 1. Donders' surface corresponding to the Fick gimbal has been sketched using the scaled co-ordinates $\bar{q}_i = \frac{q_i}{q_0}$ for $i = 1, 2, 3$. The coordinate $\bar{q}_3$ along the vertical line shows the nonzero torsion.

there corresponds (see Polpitiya et al. (2007)) a rotation matrix R (an orthogonal matrix) in $SO(3)$ given by

$$\begin{pmatrix} q_0^2 + q_1^2 - q_2^2 - q_3^2 & 2(q_1 q_2 - q_0 q_3) & 2(q_1 q_3 + q_0 q_2) \\ 2(q_1 q_2 + q_0 q_3) & q_0^2 + q_2^2 - q_1^2 - q_3^2 & 2(q_2 q_3 - q_0 q_1) \\ 2(q_1 q_3 - q_0 q_2) & 2(q_2 q_3 + q_0 q_1) & q_0^2 + q_3^2 - q_1^2 - q_2^2 \end{pmatrix}. \tag{1}$$

The corresponding map

$$rot : S^3 \to SO(3)$$

is surjective but not $1 - 1$. This is because both q and $-q$ in S^3 has the same image under 'rot'. In what follows in this paper, rigid body dynamics is written using the q-coordinates, as opposed to many other choices of coordinates for S^3.

3. RIGID BODY DYNAMICS ON $SO(3)$

We begin this section by describing the rigid body dynamics, the main ideas are already in the literature (see Isidori (1997)). The orientation of a rigid body is completely described by an orthogonal matrix R. If we assume that the angular velocity

vector is given by ω, and T is the externally applied torque, one can write down the rigid body dynamics in the 'body frame' given by

$$I\dot{\omega}(t) = S(\omega(t))I\omega(t) + T(t), \qquad (2)$$

where I is the inertia matrix [1]. The matrix $S(\omega)$ is defined as follows

$$S(\omega) = \begin{pmatrix} 0 & \omega_3 & -\omega_2 \\ -\omega_3 & 0 & \omega_1 \\ \omega_2 & -\omega_1 & 0 \end{pmatrix}. \qquad (3)$$

Assuming that the object of rotation is a homogeneous sphere, then without any loss of generality we may assume I to be an identity matrix. The equation (2) reduces to

$$\dot{\omega} = T(t). \qquad (4)$$

The angular velocity vector is related to the quaternion coordinates as follows

$$\frac{d}{dt}\begin{pmatrix} q_0 \\ q_1 \\ q_2 \\ q_3 \end{pmatrix} = \frac{1}{2}\begin{pmatrix} 0 \\ \omega_1 \\ \omega_2 \\ \omega_3 \end{pmatrix} \bullet \begin{pmatrix} q_0 \\ q_1 \\ q_2 \\ q_3 \end{pmatrix}, \qquad (5)$$

where $\bullet$ represents the quaternion product. Simplifying the above equation by carrying out the quaternion multiplication, we obtain

$$\frac{d}{dt}\begin{pmatrix} q_0 \\ q_1 \\ q_2 \\ q_3 \end{pmatrix} = \frac{1}{2}\begin{pmatrix} -(\omega_1 q_1 + \omega_2 q_2 + \omega_3 q_3) \\ \omega_1 q_0 + \omega_2 q_3 - \omega_3 q_2 \\ \omega_2 q_0 + \omega_3 q_1 - \omega_1 q_3 \\ \omega_3 q_0 + \omega_1 q_2 - \omega_2 q_1 \end{pmatrix}. \qquad (6)$$

We now choose a coordinate for the unit quaternion space as follows

$$\bar{q}_i = \frac{q_i}{q_0} \qquad (7)$$

for $i = 1, 2, 3$, and write

$$\dot{\bar{q}}_1 = \frac{1}{2}[\omega_1 + \bar{q}_3\omega_2 - \bar{q}_2\omega_3 + \bar{q}_1^2\omega_1 + \bar{q}_1\bar{q}_2\omega_2 + \bar{q}_1\bar{q}_3\omega_3], \quad (8)$$

$$\dot{\bar{q}}_2 = \frac{1}{2}[\omega_2 + \bar{q}_1\omega_3 - \bar{q}_3\omega_1 + \bar{q}_2\bar{q}_1\omega_1 + \bar{q}_2^2\omega_2 + \bar{q}_2\bar{q}_3\omega_3], \quad (9)$$

$$\dot{\bar{q}}_3 = \frac{1}{2}[\omega_3 + \bar{q}_2\omega_1 - \bar{q}_1\omega_2 + \bar{q}_3\bar{q}_1\omega_1 + \bar{q}_3\bar{q}_2\omega_2 + \bar{q}_3^2\omega_3]. \quad (10)$$

The set of equations (4), (8), (9), and (10) describe dynamics of a rigid body on $SO(3)$, in unit quaternion coordinates, under the influence of an external torque. Note that now all the quantities in state space equations (4) - (10) are expressed in the inertial frame. We are going to use these equations to address an optimal control problem in the next section.

4. RIGID BODY DYNAMICS ON *LIST*

For the eye movement problem, Listing had proposed that the axis of rotation is restricted to a plane described by the constraint

$$\bar{q}_3 = 0.$$

---

[1] In the inertial frame the form of the dynamics is identical to (2). The moment of inertia matrix, in general, changes with the orientation of the body. For a sphere rotating about the center, this is not the case.

The associated subspace of $SO(3)$ would be called *LIST*. The rigid body dynamics on *LIST* is given by

$$\dot{\bar{q}}_1 = \frac{\omega_1}{2}[1 + \bar{q}_1^2 + \bar{q}_2^2], \qquad (11)$$

$$\dot{\bar{q}}_2 = \frac{\omega_2}{2}[1 + \bar{q}_1^2 + \bar{q}_2^2], \qquad (12)$$

$$\dot{\omega}_1 = T_1, \qquad (13)$$

$$\dot{\omega}_2 = T_2, \qquad (14)$$

and

$$\omega_3 = \bar{q}_1\omega_2 - \bar{q}_2\omega_1. \qquad (15)$$

Note that the Listing's constraint appears as a constraint (15) on the angular velocity vector. It is easy to see that

$$T_3 = \bar{q}_1 T_2 - \bar{q}_2 T_1. \qquad (16)$$

Thus, the Listing's constraint forces the torque and the angular velocity vector to belong to a common plane (15), (16).

5. OPTIMAL CONTROL PROBLEMS

In this section we describe the problem of controlling a rigid body between an initial and a final state while minimizing a quadratic cost function given by

$$J = \int_0^T \frac{\alpha}{2}(T_1^2 + T_2^2 + T_3^2), \qquad (17)$$

where α is assumed to be an arbitrary constant. T is chosen as an arbitrary fixed final time. When the optimal control problem is addressed on *LIST*, the term T_3 is not used in the cost function.

5.1 Optimal control on LIST

We write down the augmented cost function given by

$$J = \int_0^T \frac{\alpha}{2}(T_1^2 + T_2^2) + p_1\left[\frac{\omega_1}{2}\left(1 + \bar{q}_1^2 + \bar{q}_2^2\right) - \dot{\bar{q}}_1\right]$$
$$+ p_2\left[\frac{\omega_2}{2}\left(1 + \bar{q}_1^2 + \bar{q}_2^2\right) - \dot{\bar{q}}_2\right]$$
$$+ p_3[T_1 - \dot{\omega}_1] + p_4[T_2 - \dot{\omega}_2] \ d\tau, \quad (18)$$

where p_1, p_2, and p_3 are co-state variables. By taking variations with respect to $\bar{q}_1$, $\bar{q}_2$, ω_1, and ω_2, we obtain the following set of co-state dynamics

$$\dot{p}_1 = -\bar{q}_1(p_1\omega_1 + p_2\omega_2), \qquad (19)$$

$$\dot{p}_2 = -\bar{q}_2(p_1\omega_1 + p_2\omega_2), \qquad (20)$$

$$\dot{p}_3 = \frac{-p_1}{2}(1 + \bar{q}_1^2 + \bar{q}_2^2), \qquad (21)$$

$$\dot{p}_4 = \frac{-p_2}{2}(1 + \bar{q}_1^2 + \bar{q}_2^2). \qquad (22)$$

Finally, taking variation with respect to the T_1 and T_2 yields the optimal controls given by

$$T_1 = -\frac{p_3}{\alpha}, \ T_2 = -\frac{p_4}{\alpha}. \qquad (23)$$

The simulation results for the optimal trajectory are shown in Fig. 2. Fig. 2 displays that externally applied torques T_1 and $T2$ drive the initial states to the final states.
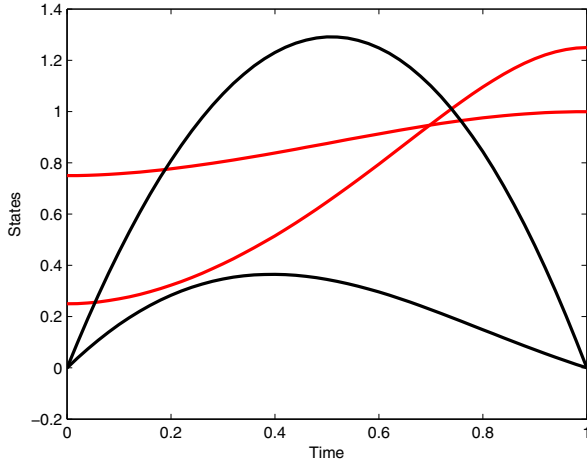
Fig. 2. Plots of state variables on LIST with initial conditions $\bar{q}_1 = 0.75$, $\bar{q}_2 = 0.25$ and final conditions $\bar{q}_1 = 1.00$, $\bar{q}_2 = 1.25$. Initial and final conditions on ω are chosen as zero and $\alpha = 10$. Black curves correspond to angular velocity vector ω, and red curves correspond to the vector $\bar{q}$.

5.2 Optimal control on $SO(3)$

We write down the augmented cost function given by

$$J = \int_0^T \frac{\alpha}{2}(T_1^2 + T_2^2 + T_3^2)$$

$$+ p_1 \left[\frac{1}{2} \left(\omega_1 + \bar{q}_3\omega_2 - \bar{q}_2\omega_3 + \omega_1\bar{q}_1^2 + \omega_2\bar{q}_2\bar{q}_1 + \omega_3\bar{q}_1\bar{q}_3 \right) - \dot{\bar{q}}_1 \right]$$

$$+ p_2 \left[\frac{1}{2} \left(\omega_2 + \bar{q}_1\omega_3 - \bar{q}_3\omega_1 + \omega_1\bar{q}_2\bar{q}_1 + \omega_2\bar{q}_2^2 + \omega_3\bar{q}_2\bar{q}_3 \right) - \dot{\bar{q}}_2 \right]$$

$$+ p_3 \left[\frac{1}{2} \left(\omega_3 + \bar{q}_2\omega_1 - \bar{q}_1\omega_2 + \omega_1\bar{q}_3\bar{q}_1 + \omega_2\bar{q}_2\bar{q}_3 + \omega_3\bar{q}_3^2 \right) - \dot{\bar{q}}_3 \right]$$

$$+ p_4[T_1 - \dot{\omega}_1] + p_5[T_2 - \dot{\omega}_2] + p_6[T_3 - \dot{\omega}_3] \ d\tau. \quad (24)$$

Variations with respect to $\bar{q}_1$, $\bar{q}_2$, $\bar{q}_3$, ω_1, ω_2, and ω_3 lead to the following co-state equations

$$\dot{p}_1 = -p_1\omega_1\bar{q}_1 - \frac{p_1}{2}\omega_2\bar{q}_2 - \frac{p_1}{2}\omega_3\bar{q}_3 - \frac{p_2}{2}\omega_3$$
$$- \frac{p_2}{2}\omega_1\bar{q}_2 + \frac{p_3}{2}\omega_2 - \frac{p_3}{2}\omega_1\bar{q}_3, \quad (25)$$

$$\dot{p}_2 = \frac{p_1}{2}\omega_3 - \frac{p_1}{2}\omega_2\bar{q}_1 - \frac{p_2}{2}\bar{q}_1\omega_1 - p_2\omega_2\bar{q}_2$$
$$- \frac{p_2}{2}\bar{q}_3\omega_3 - \frac{p_3}{2}\omega_1 - \frac{p_3}{2}\bar{q}_3\omega_2, \quad (26)$$

$$\dot{p}_3 = -\frac{p_1}{2}\omega_2 - \frac{p_1}{2}\omega_3\bar{q}_1 + \frac{p_2}{2}\omega_1 - \frac{p_2}{2}\omega_3\bar{q}_2$$
$$- \frac{p_3}{2}\bar{q}_1\omega_1 - \frac{p_3}{2}\bar{q}_2\omega_2 - p_3\bar{q}_3\omega_3, \quad (27)$$

$$\dot{p}_4 = -\frac{p_1}{2} - \frac{p_1}{2}\bar{q}_1^2 + \frac{p_2}{2}\bar{q}_3$$
$$- \frac{p_2}{2}\bar{q}_2\bar{q}_1 - \frac{p_3}{2}\bar{q}_2 - \frac{p_3}{2}\bar{q}_3\bar{q}_1, \quad (28)$$

$$\dot{p}_5 = -\frac{p_1}{2}\bar{q}_3 - \frac{p_1}{2}\bar{q}_2\bar{q}_1 - \frac{p_2}{2}$$
$$- \frac{p_2}{2}\bar{q}_2^2 + \frac{p_3}{2}\bar{q}_1 - \frac{p_3}{2}\bar{q}_3\bar{q}_2, \quad (29)$$

$$\dot{p}_6 = \frac{p_1}{2}\bar{q}_2 - \frac{p_1}{2}\bar{q}_1\bar{q}_3 - \frac{p_2}{2}\bar{q}_1$$
$$- \frac{p_2}{2}\bar{q}_2\bar{q}_3 - \frac{p_3}{2} - \frac{p_3}{2}\bar{q}_3^2. \quad (30)$$

Taking variations with respect to T_1, T_2, and T_3, we obtain the optimal controls given by

$$T_1 = -\frac{p_4}{\alpha}, \ T_2 = -\frac{p_5}{\alpha}, \ T_3 = -\frac{p_6}{\alpha}. \quad (31)$$

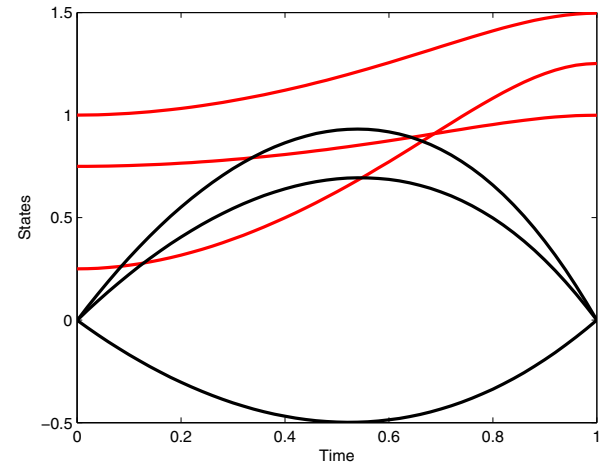The simulation results for the optimal trajectory are shown in Fig. 3.

Fig. 3. Plots of state variables on $SO(3)$ with initial conditions $\bar{q}_1 = 0.75$, $\bar{q}_2 = 0.25$, $\bar{q}_3 = 1.00$ and final conditions $\bar{q}_1 = 1.00$, $\bar{q}_2 = 1.25$, $\bar{q}_3 = 1.50$. Initial and final conditions on ω are chosen as zero and $\alpha = 10$. Black curves correspond to angular velocity vector ω, and red curves correspond to the vector $\bar{q}$.

5.3 Imposing Listing's constraint on $SO(3)$

Let us impose Listing's constraint on $SO(3)$, by augmenting cost function given by

$$J_L = \int_0^T \lambda\bar{q}_3 + \frac{\alpha}{2}(T_1^2 + T_2^2 + T_3^2)$$

$$+ p_1 \left[\frac{1}{2} \left(\omega_1 + \bar{q}_3\omega_2 - \bar{q}_2\omega_3 + \omega_1\bar{q}_1^2 + \omega_2\bar{q}_2\bar{q}_1 + \omega_3\bar{q}_1\bar{q}_3 \right) - \dot{\bar{q}}_1 \right]$$

$$+ p_2 \left[\frac{1}{2} \left(\omega_2 + \bar{q}_1\omega_3 - \bar{q}_3\omega_1 + \omega_1\bar{q}_2\bar{q}_1 + \omega_2\bar{q}_2^2 + \omega_3\bar{q}_2\bar{q}_3 \right) - \dot{\bar{q}}_2 \right]$$

$$+ p_3 \left[\frac{1}{2} \left(\omega_3 + \bar{q}_2\omega_1 - \bar{q}_1\omega_2 + \omega_1\bar{q}_3\bar{q}_1 + \omega_2\bar{q}_2\bar{q}_3 + \omega_3\bar{q}_3^2 \right) - \dot{\bar{q}}_3 \right]$$

$$+ p_4[T_1 - \dot{\omega}_1] + p_5[T_2 - \dot{\omega}_2] + p_6[T_3 - \dot{\omega}_3] + \frac{1}{2}\lambda^2\varepsilon \ d\tau, \quad (32)$$

where λ is a Lagrange's multiplier and the last term in the above equation is a penalty term, added in order to make λ smooth. The optimal control is synthesized by taking variation with respect to vectors $\bar{q}$, ω, p, T, and λ. The detailed description of co-state equations and optimal controls have been omitted since they are exactly similar to the case of optimal control on $SO(3)$. Only the equation for p_3 changes to

$$\dot{p}_3 = -\frac{p_1}{2}\omega_2 - \frac{p_1}{2}\omega_3\bar{q}_1 + \frac{p_2}{2}\omega_1 - \frac{p_2}{2}\omega_3\bar{q}_2$$
$$- \frac{p_3}{2}\bar{q}_1\omega_1 - \frac{p_3}{2}\bar{q}_2\omega_2 - p_3\bar{q}_3\omega_3 - \lambda. \quad (33)$$
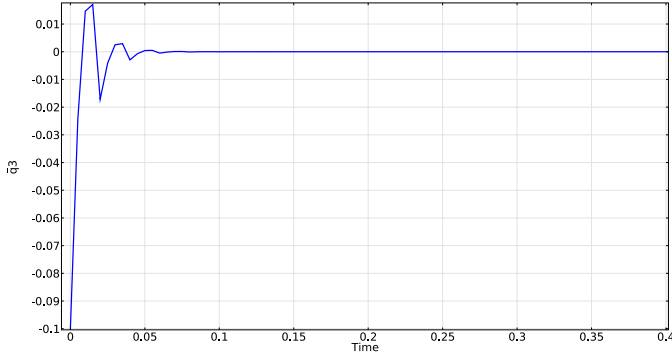
Fig. 4. Plot of $\bar{q}_3$ with $\varepsilon = 10^{-18}$ and $\alpha = 1$ when Listing's law is imposed as a constraint. Initial conditions are $\bar{q}_1 = 0$, $\bar{q}_2 = 0$, $\bar{q}_3 = -0.1$ and final conditions are $\bar{q}_1 = 1$, $\bar{q}_2 = 0$, $\bar{q}_3 = 0$. Initial and final conditions on ω are chosen as zero.
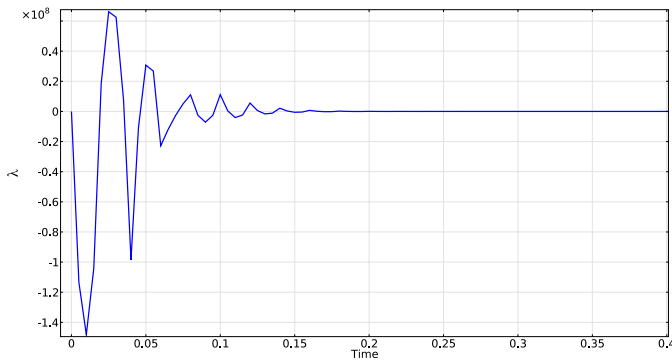

Fig. 5. For the trajectory in Fig. 4, λ is oscillating and settles down to zero. Initial and final condition on λ is chosen to be zero.

Additionally, we have an equation for λ given by

$$\varepsilon \ddot{\lambda} = \bar{q}_3. \tag{34}$$

Simulation results are sketched in Figs. 4 - 6. If the initial condition is chosen on LIST, then the trajectory always remains on LIST regardless of ε and α (not shown in the figure). But if we start away from LIST, then ε determines how quickly the trajectory follows the Listing's constraint. The Fig. 4 shows that for small ε, trajectory approaches the constraint quickly even when the initial condition is away from the constraint. In Fig. 5, an oscillatory response of λ is shown to be settling down to zero, as expected, because of zero final condition on λ. In Fig. 6, we can see oscillatory behavior of ω_2 while ω_1, $\bar{q}_1$, and $\bar{q}_2$ are smooth. The oscillatory behaviors are mainly due to lack of adequate damping in the state dynamics.

5.4 Optimal control on DOND

Two different Donders' surfaces have been used in our study. In the first, the assumption is that the movements are constrained by the FICK gimbal, and the constraint is given by

$$\bar{q}_3 + \bar{q}_1 \bar{q}_2 = 0. \tag{35}$$

The second Donders' surface was reported in Wijayasinghe et al. (2013), where the surface parameters are obtained from actual measurements of a set of human heads. Only one sample surface $S2$ has been used in this paper and is described as

$$\bar{q}_3 + 0.0087 + 0.0061\bar{q}_1 - 0.0628\bar{q}_2$$
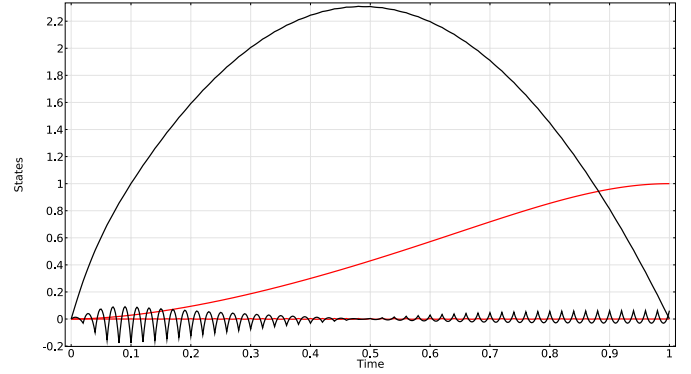$$+ 0.1434\bar{q}_1^2 + 0.0067\bar{q}_2^2 + 2.2738\bar{q}_1\bar{q}_2 = 0. \tag{36}$$

Fig. 6. Plots of $\bar{q}_1$, $\bar{q}_2$, ω_1, and ω_2 when $\bar{q}_3$ is initialized as in Fig. 4. Black and red curves correspond to angular velocity vector ω and vector $\bar{q}$ respectively. All other conditions are as in Fig. 4.

The cost function described on $SO(3)$ has the form

$$J_D = \int_0^T \lambda C + \frac{\alpha}{2}(T_1^2 + T_2^2 + T_3^2)$$
$$+ p_1 \left[\frac{1}{2} \left(\omega_1 + \bar{q}_3 \omega_2 - \bar{q}_2 \omega_3 + \omega_1 \bar{q}_1^2 + \omega_2 \bar{q}_2 \bar{q}_1 + \omega_3 \bar{q}_1 \bar{q}_3 \right) - \dot{\bar{q}}_1 \right]$$
$$+ p_2 \left[\frac{1}{2} \left(\omega_2 + \bar{q}_1 \omega_3 - \bar{q}_3 \omega_1 + \omega_1 \bar{q}_2 \bar{q}_1 + \omega_2 \bar{q}_2^2 + \omega_3 \bar{q}_2 \bar{q}_3 \right) - \dot{\bar{q}}_2 \right]$$
$$+ p_3 \left[\frac{1}{2} \left(\omega_3 + \bar{q}_2 \omega_1 - \bar{q}_1 \omega_2 + \omega_1 \bar{q}_3 \bar{q}_1 + \omega_2 \bar{q}_2 \bar{q}_3 + \omega_3 \bar{q}_3^2 \right) - \dot{\bar{q}}_3 \right]$$
$$+ p_4 [T_1 - \dot{\omega}_1] + p_5 [T_2 - \dot{\omega}_2] + p_6 [T_3 - \dot{\omega}_3] + \frac{1}{2} \lambda^2 \varepsilon \ d\tau, \tag{37}$$

where C is the appropriate constraint for FICK and $S2$ and is given by the left hand side of equations (35) and (36) respectively. The detail description of co-state equations and optimal controls under FICK have been omitted since they are exactly similar to the case of optimal control on $SO(3)$. Only the equations for p_1, p_2, and p_3 change to

$$\dot{p}_1 = -\lambda \bar{q}_2 - p_1 \omega_1 \bar{q}_1 - \frac{p_1}{2} \omega_2 \bar{q}_2 - \frac{p_1}{2} \omega_3 \bar{q}_3$$
$$- \frac{p_2}{2} \omega_3 - \frac{p_2}{2} \omega_1 \bar{q}_2 + \frac{p_3}{2} \omega_2 - \frac{p_3}{2} \omega_1 \bar{q}_3, \tag{38}$$

$$\dot{p}_2 = -\lambda \bar{q}_1 + \frac{p_1}{2} \omega_3 - \frac{p_1}{2} \omega_2 \bar{q}_1 - \frac{p_2}{2} \bar{q}_1 \omega_1$$
$$- p_2 \omega_2 \bar{q}_2 - \frac{p_2}{2} \bar{q}_3 \omega_3 - \frac{p_3}{2} \omega_1 - \frac{p_3}{2} \bar{q}_3 \omega_2, \tag{39}$$

$$\dot{p}_3 = -\lambda - \frac{p_1}{2} \omega_2 - \frac{p_1}{2} \omega_3 \bar{q}_1 + \frac{p_2}{2} \omega_1$$
$$- \frac{p_2}{2} \omega_3 \bar{q}_2 - \frac{p_3}{2} \bar{q}_1 \omega_1 - \frac{p_3}{2} \bar{q}_2 \omega_2 - p_3 \bar{q}_3 \omega_3. \tag{40}$$

Additionally, by taking variation with respect to λ, we obtain the following constraint equation.

$$\varepsilon \ddot{\lambda} = \bar{q}_3 + \bar{q}_1 \bar{q}_2. \tag{41}$$

The detail description of co-state equations and optimal controls under $S2$ have also been omitted since they are exactly similar to the case of optimal control on $SO(3)$. Only the equations for p_1, p_2, and p_3 change to

$$\dot{p}_1 = -\lambda(0.0061+0.2868\bar{q}_1+2.2738\bar{q}_2) - p_1\omega_1\bar{q}_1 - \frac{p_1}{2}\omega_2\bar{q}_2$$
$$- \frac{p_1}{2}\omega_3\bar{q}_3 - \frac{p_2}{2}\omega_3 - \frac{p_2}{2}\omega_1\bar{q}_2 + \frac{p_3}{2}\omega_2 - \frac{p_3}{2}\omega_1\bar{q}_3, \quad (42)$$

$$\dot{p}_2 = -\lambda(-0.0628+0.0134\bar{q}_2+2.2738\bar{q}_1) + \frac{p_1}{2}\omega_3 - \frac{p_1}{2}\omega_2\bar{q}_1$$
$$- \frac{p_2}{2}\bar{q}_1\omega_1 - p_2\omega_2\bar{q}_2 - \frac{p_2}{2}\bar{q}_3\omega_3 - \frac{p_3}{2}\omega_1 - \frac{p_3}{2}\bar{q}_3\omega_2, \quad (43)$$

$$\dot{p}_3 = -\lambda - \frac{p_1}{2}\omega_2 - \frac{p_1}{2}\omega_3\bar{q}_1 + \frac{p_2}{2}\omega_1$$
$$- \frac{p_2}{2}\omega_3\bar{q}_2 - \frac{p_3}{2}\bar{q}_1\omega_1 - \frac{p_3}{2}\bar{q}_2\omega_2 - p_3\bar{q}_3\omega_3. \quad (44)$$

The constraint equation for $S2$ is given by

$$\varepsilon\ddot{\lambda} = \bar{q}_3 + 0.0087 + 0.0061\bar{q}_1 - 0.0628\bar{q}_2$$
$$+ 0.1434\bar{q}_1^2 + 0.0067\bar{q}_2^2 + 2.2738\bar{q}_1\bar{q}_2. \quad (45)$$

Fig. 7 shows that for small ε, trajectory follows the constraint quickly even when the initial condition is away from the constraint.
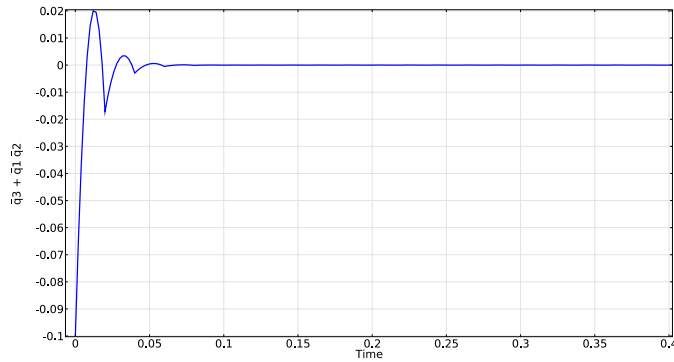

Fig. 7. Plot of $\bar{q}_3 + \bar{q}_1\bar{q}_2$ with $\alpha = 1$ and $\varepsilon = 10^{-20}$ under FICK constraint. Initial conditions are $\bar{q}_1 = 0$, $\bar{q}_2 = 0$, $\bar{q}_3 = -0.1$ and final conditions $\bar{q}_1 = 1$, $\bar{q}_2 = 0$, $\bar{q}_3 = 0$. Initial and final conditions on ω are chosen as zero.
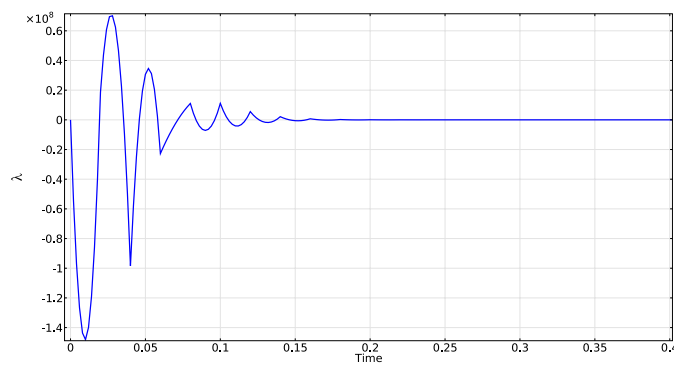

Fig. 8. For the trajectory in Fig. 7, λ is oscillating and settles down to zero. Initial and final condition on λ is chosen to be zero.

Fig. 10 shows that under the $S2$ constraint, trajectory follows the constraint quickly, though not as quickly as in Fig. 7.

In Fig. 9, we can see an oscillatory behavior of ω_1 and ω_2 while $\bar{q}_1$ and $\bar{q}_2$ are smooth. The plots of states under $S2$ constraint also show the same behavior as LIST and FICK (not shown in the figures). Figs. 8 and 9 show the oscillatory response of λ as in Fig. 5.
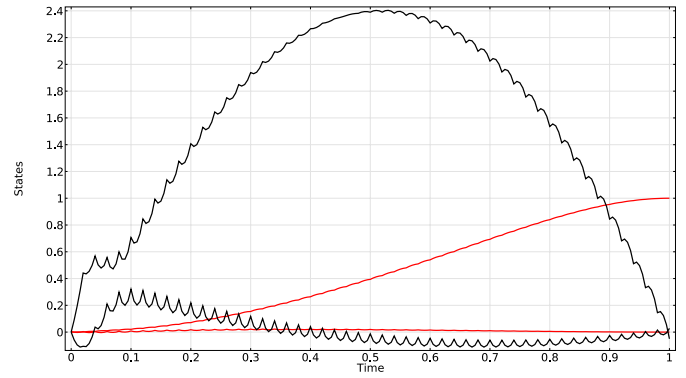

Fig. 9. Plots of $\bar{q}_1$, $\bar{q}_2$, ω_1, and ω_2 under FICK constraint when the states are initialized away from the constraint. Black and red curves correspond to angular velocity vector ω and vector $\bar{q}$ respectively. All the conditions are same as in Fig. 7.
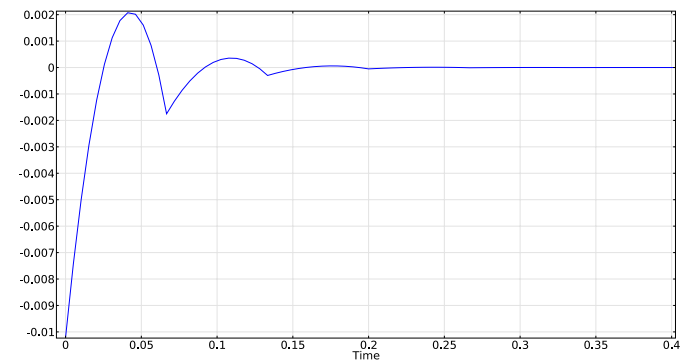

Fig. 10. Plot of left hand side of the equation (36) with $\varepsilon = 10^{-25}$ and $\alpha = 1$ under $S2$ constraint. Initial conditions $\bar{q}_1 = 0$, $\bar{q}_2 = 0$, $\bar{q}_3 = -0.0187$ and final conditions $\bar{q}_3 = -0.2132$, $-\bar{q}_1 = 1$, $\bar{q}_2 = 0$. Initial and final conditions on ω are chosen as zero.
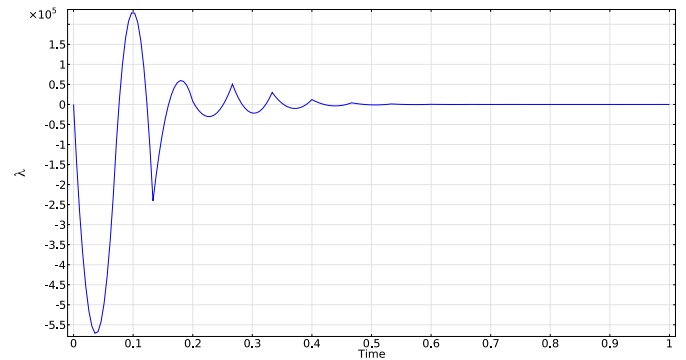

Fig. 11. For the trajectory in Fig. 10, λ is oscillating and settles down to zero. Initial and final condition on λ is chosen to be zero.

6. DISCUSSION

In this paper we have introduced a new parametrization, called q-parametrization, to describe a rigid body dynamics under externally applied torques T_1, T_2, and T_3. We have also assumed that the rigid body is a homogeneous sphere, rotating around its center. Thus, without any lost of generality, we assume that the moment of inertia is the identity matrix. All state equations have been written in the inertial frame.

In the past, Ghosh and Wijayasinghe (2012b), Wijayasinghe et al. (2013), we have used Axis-Angle parametrization and Tait-Bryan parametrization to describe eye movement and head
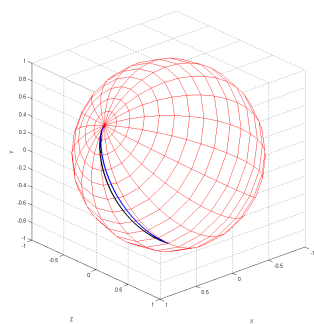
(a) Gaze trajectory.
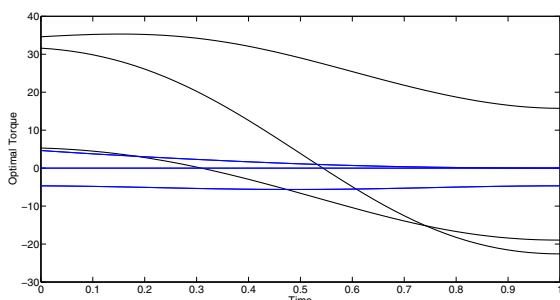
(b) External torques.

Fig. 12. Optimal curves starting from the gaze/pointing direction $(0\ 0\ 1)^T$ (frontal) and ending at $(0\ -1\ 0)^T$ (straight downward) under LIST and FICK constraints imposed on SO(3) and plot of corresponding optimal torques. Blue and Black correspond to LIST and FICK respectively. Initial and final conditions on ω have been chosen as zero, $\alpha = 1$, and $\varepsilon = 10^{-4}$.

movement under the Listing's and Donders' constraint respectively. The Axis-Angle parametrization has a singularity at the frontal gaze direction, while the Tait-Bryan parametrization has singularities at straight up/down gaze directions. For the q-parametrization, proposed in this paper, there are no singularities. It is therefore possible to simulate optimal trajectories that start at the frontal gaze direction and terminate at the straight down gaze direction. This has been demonstrated in Fig. 12a under Listing's and Fick's constraints. As an additional point, we note from Fig. 12a that the optimal trajectories are close although the corresponding optimal torques, shown in Fig. 12b, are not. We also remark that since the states are initialized on the corresponding constraints, the value of ε in the simulation shown in Fig. 12 is not as small as what was chosen in Fig. 4. Since the value of ε is chosen to be large, the state responses in this simulation do not show any oscillatory behavior, evident from the gaze trajectories in Fig. 12a.

ACKNOWLEDGEMENTS

REFERENCES

M. Ceylan, D. Y. P. Henriques, D. B. Tweed, and J. D. Crawford. Task-dependent costraints in motor control: Pinhole goggles make the head move like an eye. *The Journal of Neuroscience*, 20(7):2719–2730, April. 2000.

F. C. Donders. Beiträge zur lehre von den bewegungen des menschlichen auges. *Holländische Beiträge zu den anatomischen und physiologischen Wissenschaften*, 1:104–145, 1848. Press, 1996.

B. K. Ghosh and I. Wijayasinghe. Dynamics of human head and eye rotations under Donders' constraint. *IEEE Trans. on Aut. Contr.*, 57(10):2478–2489, Oct. 2012a.

B. K. Ghosh and I. Wijayasinghe. Dynamics of human head and eye rotations under Donders' constraint. *IEEE Trans. on Automat. Contr.*, 57(10):2478–2489, Oct. 2012b.

B. Glenn and T. Vilis. Violations of listing's law after large eye and head gaze shifts. *J. Neurophysiol.*, 68:309–318, 1992.

H. Von Helmholtz. *Handbuch der Physiologischen Optik.* Number 3, Leopold Voss, Hamburg & Leipzig, 1910. Leipzig: Vos., 3rd edition, 1866.

A. Isidori. *Nonlinear Control Systems.* Springer-Verlag, New York, NY, third edition, 1997.

J. B. Listing. *Beiträge zur physiologischen Optik.* Göttinger Studien, Vandenhoeck und Ruprecht, Göttingen, 1845.

W. P. Medendorp, B. J. M. Melis, C. C. A. M. Gielen, and J. A. M. Van Gisbergen. Off-centric rotation axes in natural head movements: implications for vestibular reafference and kinematic redundancy. *J. Neurophysiology*, 79:2025–2039, 1998.

H. Misslisch, D. Tweed, and T. Vilis. Neural constraints on eye motion in human eye-head saccades. *J. Neurophysiol.*, 79: 859–869, 1998.

A. D. Polpitiya, W. P. Dayawansa, C. F. Martin, and B. K. Ghosh. Geometry and control of human eye movements. *IEEE Trans. on Aut. Contr.*, 52(2):170–180, Feb. 2007.

P. Radau, D. Tweed, and T. Vilis. Three dimensional eye head and chest orientations following large gaze shifts and the underlying neural strategies. *J. Neurophysiol.*, 72:2840–2852, 1994.

D. Straumann, T. Haslwanter, M. C. Hepp-Reymond, and K. Hepp. Listing's law for the eye, head, and arm movements and their synergistic control. *Exp. Brain Res.*, 86:209–215, 1991.

M. Theeuwen, L. E. Miller, and C. C. A. M. Gielen. Are the orientations of the head and arm related during pointing movements? *J. Motor Behav.*, 25:242–250, 1993.

D. Tweed, B. Glenn, and T. Vilis. Eye-head coordination during large gaze shifts. *J. Neurophysiol.*, 73:766–779, 1995.

I. Wijayasinghe, J. Ruths, U. Büttner, B. K. Ghosh, S. Glasauer, O. Kremmyda, and Jr-Shin Li. Potential and optimal control of human head movement using Tait-Bryan parametrization. *Automatica*, 2013.